Renewable Energy 214 (2023) 185–193

Contents lists available at ScienceDirect

Renewable Energy

journal homepage: www.elsevier.com/locate/renene

Numerical study for nonlinear hydrodynamic coefficients of an asymmetric wave energy converter

Haeng Sik Ko [a], Sunny Kumar Poguluri [b], Jeong-Heon Shin [b], Yoon Hyeok Bae [b,*]

[a] Coastal Development and Ocean Energy Research Center, Korea Institute of Ocean Science and Technology, 49111, Busan, Republic of Korea
[b] Department of Mechanical & System Design Engineering, Hongik University, 04066, Seoul, Republic of Korea

ARTICLE INFO

Keywords:
Asymmetric wave energy converter
Reynolds-averaged Navier-Stokes equation
Response amplitude operator
Hydrodynamic coefficients
Nonlinear effect

ABSTRACT

In this study, the nonlinear dynamic behavior of an asymmetric Wave Energy Converter (WEC) was studied on a 1/11-scale model based on a numerical and experimental method in a regular wave field. The numerical analysis involved both frequency-domain and time-domain solutions. The frequency-domain solution was based on linear potential flow theory using the WAMIT® model whereas the time-domain solution was based on the Reynolds-Averaged Navier-Stokes (RANS) equation using the OpenFOAM® model. The pitch response amplitude operators obtained from the numerical results were compared with experimental data. Additionally, the nonlinear dynamic behavior of the asymmetric WEC due to various wave heights and periods obtained through the experiments were compared with the OpenFOAM results. Wave excitation moments and hydrodynamic coefficients based on the linear solution approach were separately obtained for the fixed asymmetric WEC induced by waves and the forced oscillating motion with OpenFOAM. Moreover, frequency-domain solutions based on linear potential flow theory were obtained in order to ascertain the nonlinear effects observed in the OpenFOAM results. It was found that a higher motion amplitude could be attributed to nonlinear hydrodynamic coefficients on the asymmetric WEC calculated by the forced oscillation motion of the RANS-based solution.

1. Introduction

Interest in renewable energy has been increasing due to the negative impacts of energy produced from fossil fuels, such as environmental pollution and climate change, as well as the potential risks of nuclear energy, for example waste disposal. Harvesting ocean wave energy represents a potentially rich source of renewable energy, however this approach has not been widely commercialized [1,2]. The Edinburgh Duck wave energy converter (WEC), which is a typical pitching WEC, achieves an energy efficiency of about 90% due to the asymmetric shape of the incident wave direction and the transmission wave direction [3]. In order to maximize the efficiency of the Edinburgh Duck WEC, various design parameters (cross-sectional shape, draft, center of gravity, etc.) should be determined according to the wave climates in deployment areas. Parametric studies have been carried out to investigate the performance of the Edinburgh Duck WEC [4,5]. Additionally, recent effort has been made by Weptos A/S (Fredericia, Denmark) to pre-commercialize an arrayed wave energy converter in which multiple Edinburgh ducks are coupled to a weathervaning platform to enhance the energy-extraction efficiency [6].

The hydrodynamic behavior of an Edinburgh Duck WEC is initially analyzed based on linear potential flow theory, where the numerical theory does not take the viscous effect into account and thus makes the behavior near the resonance period excessive [7]. Liu et al.[8] and Liu [9] attempted to enhance the linear theory by implementing novel numerical techniques and methodologies to improve the computational accuracy and efficiency, specifically targeting issues related to the free-surface Green's function in finite water depth. The implementation, has been made publicly available for all users, enabling them to investigate any type of WEC device. Despite efforts to enhance the linear theory, frequency domain solutions based on linear models continue to suffer from a tendency to overestimate the response of wave energy converter (WEC) devices. To account for the viscous effects, some past researchers have conducted numerical analysis of WECs in different ways. Some have incorporated external viscous damping, while others have included the drag-force term in their linear evaluation process. However, this requires additional work, namely a free decay test [10–13] or the calculation of the drag coefficients [14–16] of a WEC using computational fluid dynamics (CFD) or a model experiment. Since the above methods use parameterized values, there are limitations in

* Corresponding author. Hongik University, 94, Wausan-ro, Mapo-gu, Seoul, 04066, Republic of Korea.
E-mail address: yhbae@hongik.ac.kr (Y.H. Bae).

https://doi.org/10.1016/j.renene.2023.06.023
Received 27 May 2022; Received in revised form 24 April 2023; Accepted 8 June 2023
Available online 8 June 2023
0960-1481/© 2023 Elsevier Ltd. All rights reserved.

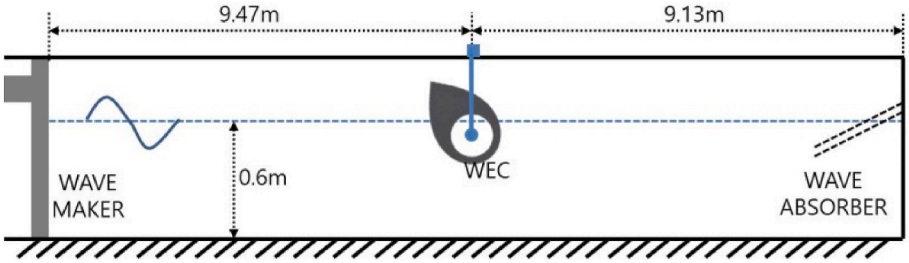

Fig. 1. Sketch of the experimental wave tank. WEC: Wave Energy Converter.

application to fully nonlinear viscous effects.

Some researchers have employed weakly nonlinear time domain models to address the large motion response of WECs. Lawson et al. [17] developed a capability to estimate buoyancy and Froude-Krylov forces from the instantaneous position of a WEC device in WEC-Sim, resulting in well-captured relevant physics of the WEC's large motions. Similarly, Zurkinden et al. [14] used a cubic polynomial function to consider the nonlinear hydrostatic restoring moment in a 3D WEC with the viscous drag force taken into account, and their results were able to capture the relevant dynamics of the WEC up to a wave steepness of 0.04. Wang et al. [18] developed a weakly nonlinear time-domain model called SIMDYN that included nonlinear Froude-Krylov forces into the linear solution and tested against the point type wave absorber, resulting in reasonably good agreement with experimental tests in both regular and irregular wave conditions. Giorgi et al. [19] proposed an alternative analytical approach that considered the nonlinear Froude-Krylov model in studying the nonlinear hydrodynamic behavior of a pitch-type WEC, which demonstrated the advantages of the developed analytical model in handling non-zero mean free-decay, nonlinear response, and dynamic excitation with consideration of the actual instantaneous wetted surface. Recent past, Chandrasekaran and Sricharan [20] used linear and weakly nonlinear model ANSYS AQWA and WEC-Sim, respectively, to investigate a new multi-body floating WEC. The results of the linear domain solution (in frequency and time) overestimated the extracted power, while the weakly nonlinear model showed the extracted power to be half of that of the linear time-domain model. However, it is evident from this review of weakly nonlinear models that they can only handle a certain degree of the nonlinear hydrodynamic behavior of WECs and still fall short of considering their full nonlinear and complex motion response.

Numerical studies of the nonlinear dynamic behavior of WECs have been conducted using CFD considering high nonlinearity and viscosity by using parallel processing technology or Graphics Processing Units (GPUs). In particular, the OpenFOAM® (Open-Source Field Operation and Manipulation) CFD model, which is based on an open-source library, is widely used for the numerical analysis of WECs. Eskilsson et al. [21] used OpenFOAM to estimate overtopping discharge in a floating WEC. Additionally, Schmitt and Elsaesser [22] simulated an oscillating surge WEC induced by regular waves using an arbitrary mesh interface technique without re-meshing. Furthermore, Ko et al. [23] investigated optimal performance of a horizontal eccentric cylinder-type WEC, both experimentally and numerically. The authors found that the response of the horizontal eccentric cylinder-type WEC is nonlinear, even though the incident wave steepness is linear.

OpenFOAM can be utilized as a fully nonlinear viscous numerical model to obtain various hydrodynamic coefficients, such as wave excitation forces, added mass, and damping. The wave excitation forces are calculated by integrating the dynamic pressure and shear stress generated by regular waves over the asymmetric WEC in fixed mode. On the other hand, the added mass and damping coefficients are derived by forcing the WEC and converting the resulting time series into the frequency domain using Fourier series transform. This approach is similar to the one adopted in the present study, and it can also accurately account for all viscous effects. Hydrodynamic coefficients for various shapes of WEC determined by the forced oscillating motion have been experimentally determined with different oscillation amplitudes [24]. Moreover, numerical studies have used CFD code to investigate hydrodynamic coefficients by the forced oscillating roll motion of floating objects [25]. Davidson et al. [26] utilizedCFD models to obtain hydrodynamic coefficients and hydrostatic coefficient from a free decay test performed on a cylindrical body with a symmetric shape. They combined the CFD models with a boundary element method (BEM)-type model to reduce computational effort. They found that the dissipative effects are all different by the CFD model. Ko et al. [27] investigated the effect of nonlinear dynamic behavior of asymmetrical pitching-type WEC even induced by the linear wave condition. They found that the radiation moment becomes nonlinear as the forced-oscillation

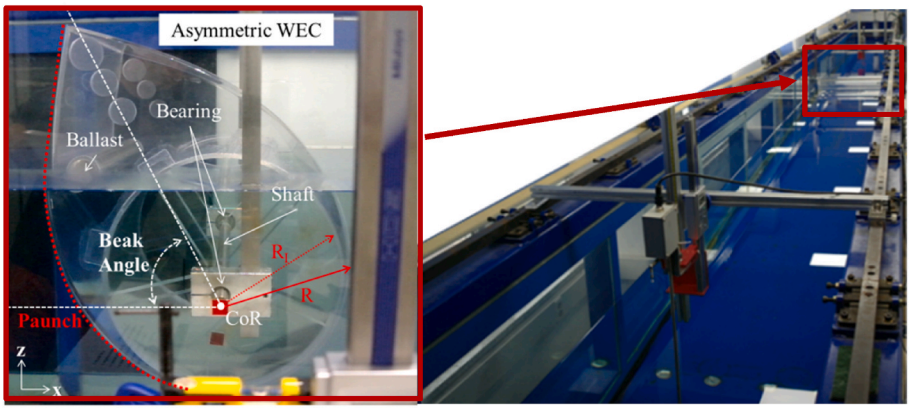

Fig. 2. Annotated photograph of the asymmetric WEC (1/11 scale) and full experimental setup used in this study.

Table 1
Specifications of the asymmetric WEC used in this study (1/11 scale).

Material	Acrylic (WEC), Steel bar (Ballast weight)
Beak Angle [deg]	60
Stern Radius (R) [m]	0.182
Inner Hollow Radius (R_I) [m]	0.17
Draft [m]	0.3275
Width [m]	0.4545
CoGx,z from CoR [m]	(–0.093, 0.0998)
Mass [kg]	13.6505
Moment of Inertia (w.r.t. CoG) [kg·m^2]	0.4934
Moment of Inertia (w.r.t. CoR) [kg·m^2]	0.7479

Table 2
The incident wave conditions.

H [m]	T [s]						
0.01 0.03	1.30	1.40	1.50	1.55	1.60	1.70	1.80

Note: H: wave height; T: wave period.

amplitude is higher through two-dimensional CFD simulation.

The present study highlights the investigation of the nonlinear dynamic behavior of an asymmetric WEC and estimate important hydrodynamic coefficients such as added mass, damping, and wave excitation moments. To achieve this, the study employs a linear solution approach using CFD simulations. The approach involves integrating dynamic pressure and shear stress to obtain the wave excitation moments with the WEC fixed, while Fourier transformation is used to convert time series data from the forced WEC into the frequency domain to obtain added mass and damping. By employing this linear solution approach, a direct comparison can be made between the nonlinear (using CFD) and linear (using a well-established linear potential model theory) methods in assessing the dynamic behavior of the asymmetric WEC. This comparison also helps to gain a deeper understanding of the complex interaction behavior of the asymmetric WEC.

The paper is organized as follows: Section 2 provides an overview of the experimental setup, where experiments were conducted on a 1/11-scale model of an optimized asymmetric wave energy converter based on the proposed Edinburgh duck shape in the sea to the west of Jeju Island, Republic of Korea [28–31]. Section 3 discusses the 3D numerical simulations performed using OpenFOAM v1812 to analyze the hydrodynamic behavior of the asymmetrical WEC induced by regular waves. In Section 4, the results and discussion are presented, including the comparison of pitch response amplitude operators (RAOs) due to different wave heights with experimental results, spectral analysis of pitch excursion induced by regular waves to analyze nonlinear hydrodynamic behavior, and the use of a linear solution approach to separately obtain wave excitation moments and hydrodynamic coefficients with respect to nonlinear dynamic behavior considering nonlinear viscous effects. Additionally, wave excitation moments with a constraint of all degrees of freedom of the asymmetric WEC and hydrodynamic coefficients (added moment of inertia and damping) induced by forced oscillation are computed using both the OpenFOAM model based on the Reynolds-Averaged Navier-Stokes equation and the WAMI T[32] model based on linear potential theory, and the results of these two models are compared. Moreover, instantaneous snapshots of the vorticity field and dynamic pressure distribution at the maximum and minimum moment due to forced oscillation are compared for different motion amplitudes. Finally, Section 5 provides conclusions based on the findings of the study.

Table 3
A comparison of the root-mean-square difference (RMSD) values determined by the grid convergence test.

Mesh resolution	dx/dz (m)	Mesh number (in length)	Mesh number (in height)	H_{RMSD} (in time)	H_{RMSD} (in space)
Coarse	0.02/0.01	121	3	0.00090	0.00114
Medium	0.01/0.005	242	6	0.00077	0.00113
Fine	0.005/0.0025	483	12	0.00075	0.00113

2. Experimental setup of the 1/11-scale model

The asymmetric WEC experimental model was fabricated at a scale ratio of 1/11. A real-scale prototype optimized with a significant wave height (H_s) of 2 m and a peak period (T_p) of 6.5 s in the sea to the west of Jeju island considering various design parameters, such as cross-sectional shape, draft, and center of gravity (CoG), was proposed [28]. Fig. 1 shows a cross-sectional view of the 1/11-scale prototype deployed in a two-dimensional wave tank (length: 20 m; width: 0.8 m; height: 1.0 m) at Jeju National University. Waves were generated via a piston-type wave maker and the waves were absorbed at the end of the water tank by inclined double-layered perforated stainless-steel plates.

The asymmetric WEC was suspended from a stiff bridge with the help of vertical rods that were fixed using clamps in the wave flume. These rods allowed for maintaining the required draft. A shaft, which passed through the center of rotation (CoR) of the rotor, connected both ends of the shaft to the vertical rods and enabled the WEC to move up and down around its CoR. To ensure that the asymmetric WEC could pitch smoothly about its CoR, a bearing mechanism was employed to reduce friction between the shaft and the vertical rods. To measure the pitch excursions caused by the incident waves, an image tracking technique was employed. Two red square marks were placed on the WEC, with one

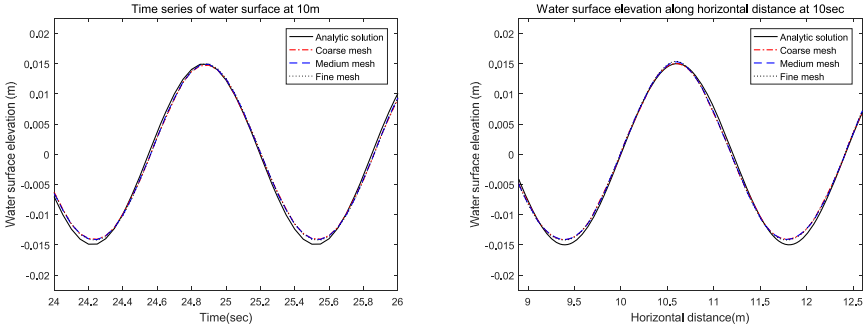

Fig. 3. A comparison of wave elevations at different grid resolutions. (a) Time series of wave elevation. (b) Variation of wave elevation along the horizontal direction.

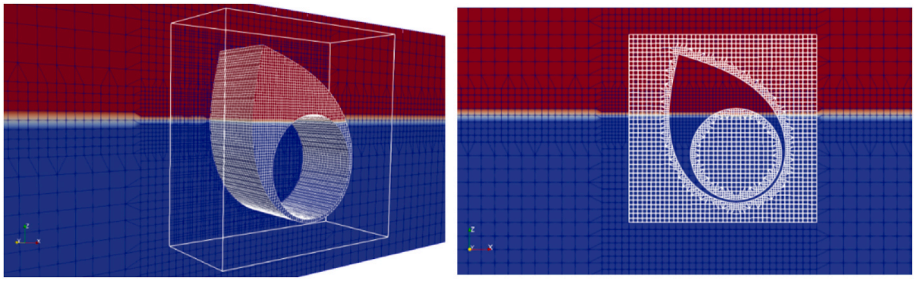

Fig. 4. Three-dimensional and cross-sectional grid system near the WEC showing the fixed mesh and overset mesh (dynamic) region (white color).

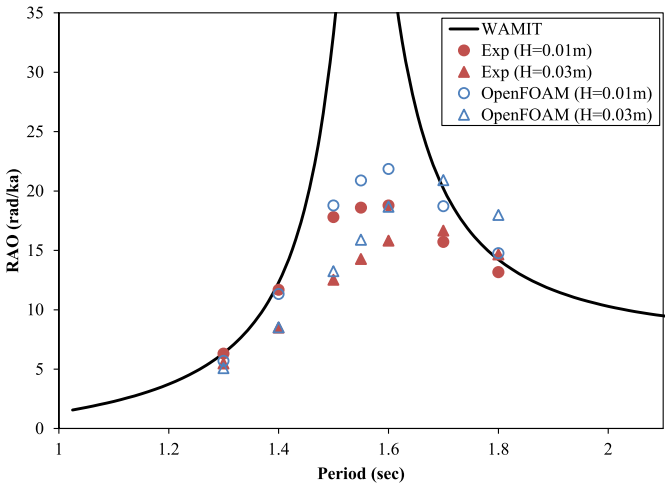

Fig. 5. Comparison of response amplitude operators (RAOs) for pitch motion.

fixed at the shaft and the other moving along with the WEC (as depicted in Fig. 2). To ensure accurate pitch excursion measurement of the asymmetric WEC, a high-quality video is necessary. Two important factors that impact the quality of the recording are the frame rate and pixel count. While a high-specification video camera can offer superior accuracy, it can also lead to longer computational processing time. Therefore, selecting the optimal balance between accuracy and processing speed is a paramount issue in the image tracking method. For this study, we utilized a camera with a resolution of 1280 × 720 and a frame rate of 240fps, and performed image processing using MATLAB software. The accuracy of the image processing technique adopted in this study is assessed and compared with the CFD simulations in the following section. Table 1 shows the detailed specifications of the asymmetric WEC. Table 2 summarizes the selected incident wave conditions based on the test field of the west coast of Jeju Island.

3. Numerical analysis

The overInterDyMFoam solver—one of the solvers in OpenFOAM which is used for solving multi-phase flow with dynamic mesh motion

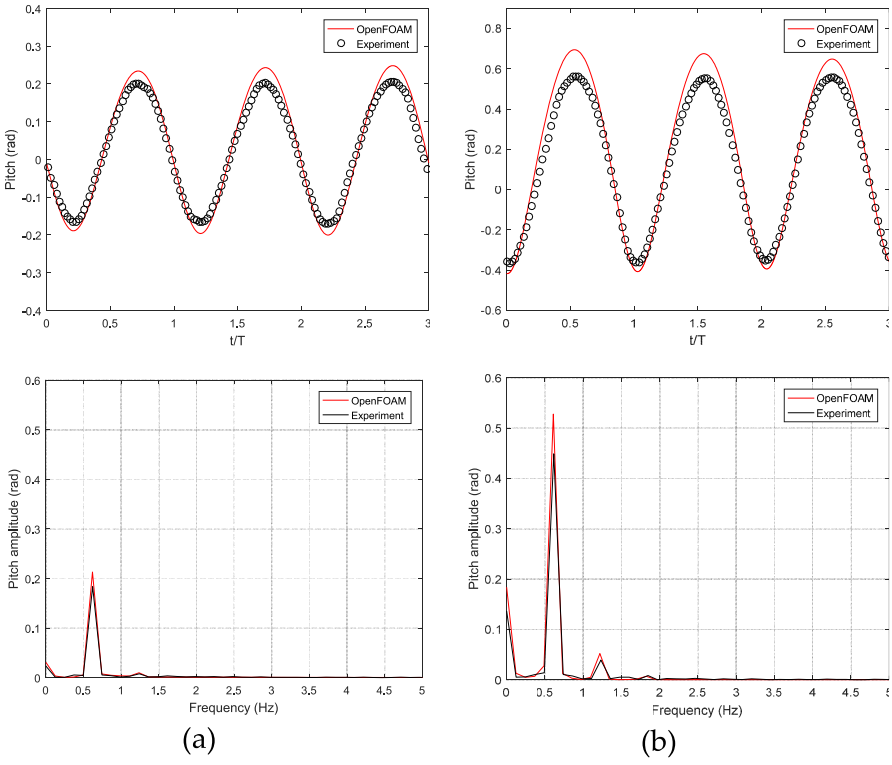

Fig. 6. Comparison of time series (top) and spectral analysis (bottom) of pitch motion. (a) $H = 0.01\,m$; $T = 1.60\,sec$. (b) $H = 0.03\,m$; $T = 1.60\,sec$.

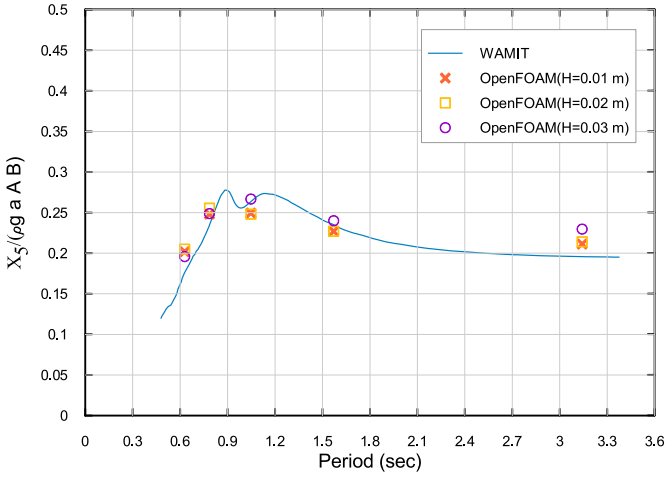

Fig. 7. Comparison of the wave excitation moments (X_5) calculated using the potential flow solution (WAMIT) and the OpenFOAM solution. The parameters ρ, g, a, and A and B are the water density, gravitational acceleration, wave amplitude, and the submerged section area and breadth of the asymmetric WEC, respectively.

through an overset mesh—was used to analyze the interaction between the asymmetric WEC and the fluid. The RANS equation discretized by the finite volume method (FVM) was used for the equation of motion of the fluid.

$$\frac{\partial \overline{u}_j}{\partial x_j} = 0 \tag{1}$$

$$\frac{\partial \overline{u}_i}{\partial t} + \overline{u}_j \frac{\partial \overline{u}_i}{\partial x_j} = \frac{\partial}{\partial x_j}\left[\nu_{eff}\left(\frac{\partial \overline{u}_i}{\partial x_j} + \frac{\partial \overline{u}_j}{\partial x_i}\right)\right] - \frac{1}{\rho}\frac{\partial}{\partial x_i}\left(\overline{p} + \frac{2}{3}\rho k\right) \tag{2}$$

where $\overline{u}$ is the average fluid velocity, ρ is the fluid density, $\overline{p}$ is the mean fluid pressure, and ν_{eff} is the effective kinematic constant calculated as the sum of the molecular viscosity (ν) and the turbulent kinematic viscosity (ν_t). In this study, the Re-Normalization Group (RNG) k-ε turbulence model by Yakhot et al. [33] was used for the analysis of turbulent flow. The equations of motion of the asymmetric WEC based on the velocity and pressure obtained by solving Equations (1) and (2) for fluid flow analysis are as follows:

$$M_T = \int_S \left(M_{ext} + M_{flow}\right) ds = J\ddot{\theta} \tag{3}$$

where M_T is total moment of the WEC; M_{ext} is the external moment of the WEC due to gravity; M_{flow} is the buoyancy moment of the WEC due to pressure or viscosity; J is the moment of inertia of the WEC; the dot represents the time derivative; and θ is the rotational excursions of the WEC.

The integration of functionality produced by Higuera et al. [34] for wave generation and absorption was used. For wave generation, a specific boundary condition calculated using wave theory formula was

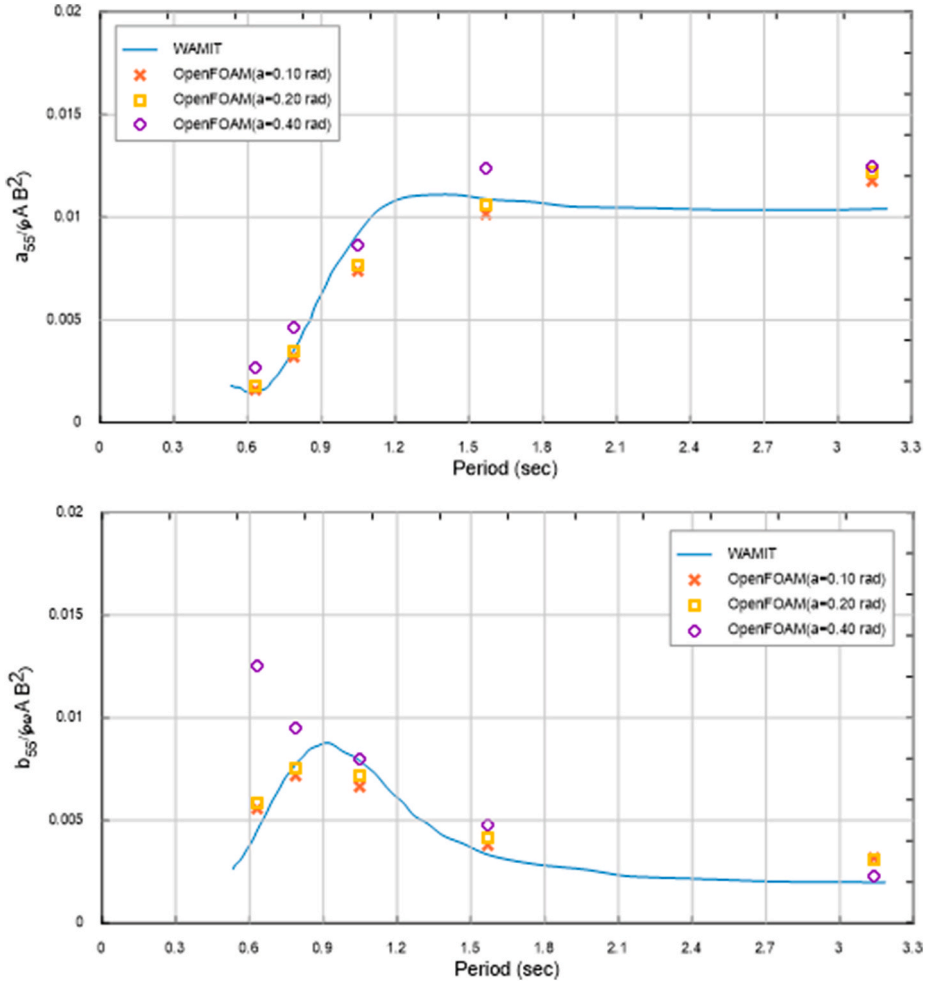

Fig. 8. Comparison of added moment of inertia (top) and damping coefficients (bottom) obtained from the potential flow solution (WAMIT) and the OpenFOAM solution.

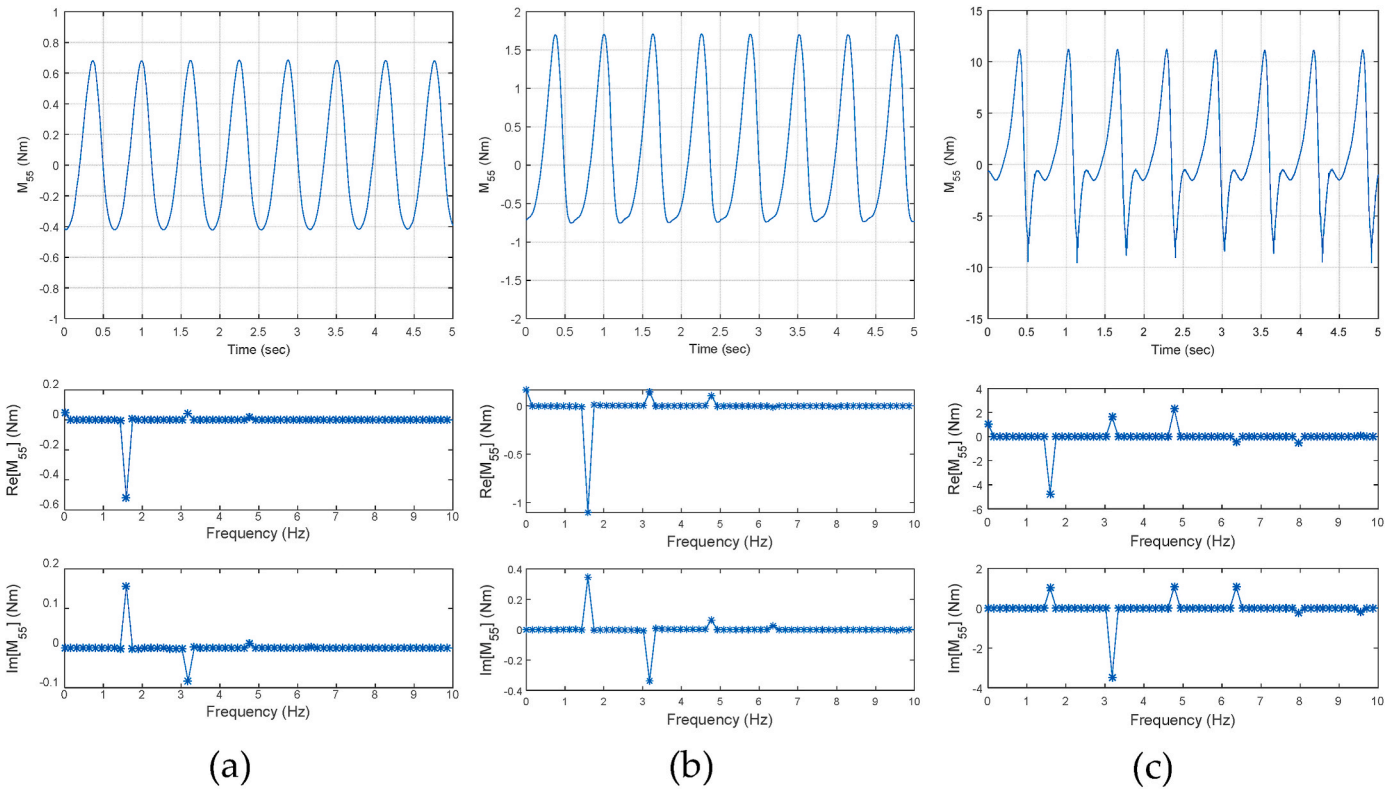

Fig. 9. A comparison of time series (top) and spectral analyses of the real part (middle) and imaginary part (bottom) of the moment due to the forced oscillation with different motion amplitudes. (a) $a = 0.1$ rad, $\omega = 10$ rad/s. (b) $a = 0.2$ rad, $\omega = 10$ rad/s. (c) $a = 0.4$ rad, $\omega = 10$ rad/s.

input into OpenFOAM. Active wave absorption based on the linear shallow-water wave theory of Schaffer and Klopman [35] was applied to control the reflected wave.

An overset mesh technique was adopted to analyze the moving body without re-meshing by creating a separate grid domain for the background and the moving body. The mesh zones were composed of a background mesh, a fixed mesh region, and an overlapped mesh region. The overset patch regions were interpolated from the solution mesh using the governing equation.

4. Results and discussion

4.1. Grid convergence test

A grid convergence test was carried out to assess the accuracy and efficiency of wave generation and propagation. The most stringent case with the highest wave steepness ($ka = 0.039$) was selected for the grid convergence test. Fig. 3 shows a comparison of the time series of water surface elevation at the middle of the wave flume where the WEC was deployed and the spatial distribution of the water surface elevation at

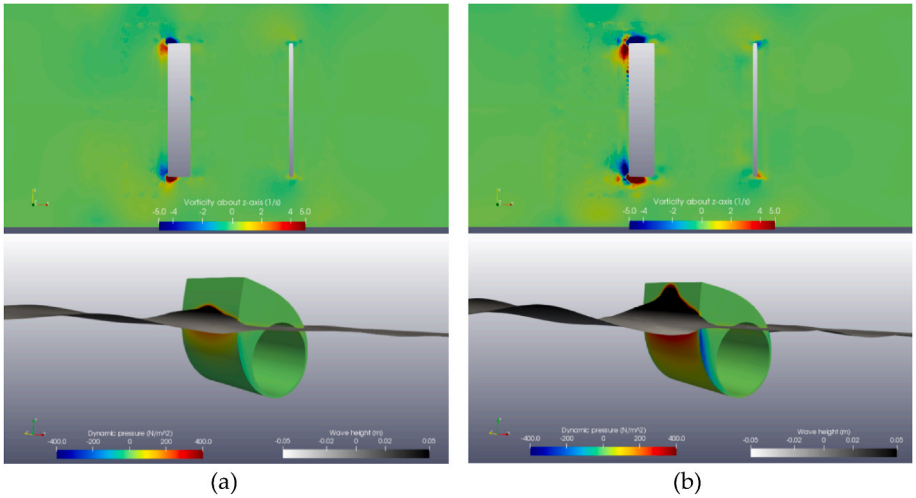

Fig. 10. A comparison of the instantaneous vorticity distribution about the z-axis in the plane z = 0 (top) and the dynamic pressure distribution on the WEC with wave height (bottom) at the negative maximum forced oscillation for different motion amplitudes. (a) $a = 0.2$ rad, $\omega = 10$ rad/s. (b) $a = 0.4$ rad, $\omega = 10$ rad/ s.

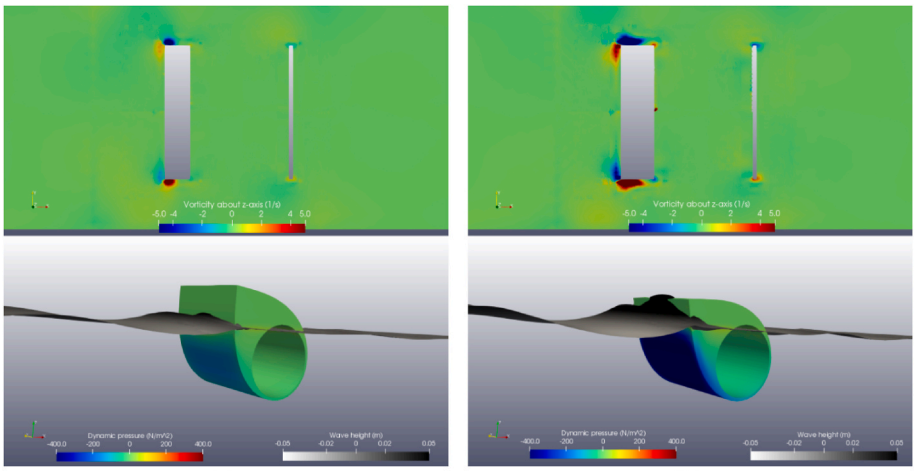

Fig. 11. A comparison of the instantaneous vorticity distribution about the z-axis in the plane z = 0 (top) and the dynamic pressure distribution on the WEC with wave height (bottom) at the positive maximum forced oscillation for different motion amplitudes. (a) $a = 0.2$ rad, $\omega = 10$ rad/s. (b) $a = 0.4$ rad, $\omega = 10$ rad/ s.

20 *sec* with different grid resolutions (coarser, medium, and finer) with the Airy wave theory. The theoretical solution and the numerical solutions were compared for a total of 10 wave cycles using the root-mean-square difference (RMSD), and the results are shown in Table 3. The results show that the finer the grid resolution, the lower the RMSD. Considering the efficiency and accuracy of the computational calculation, the medium grid resolution was selected for the following numerical analysis in this study.

As shown in Fig. 4, based on the results of the grid convergence test, the final grid resolution was chosen to be higher around the asymmetric WEC and near the free water surface in order to improve the efficiency of the numerical calculation. A refinement ratio of 0.005/0.0025, which is half the size of the medium grid values as used in Fig. 3. Since we employed an overset mesh to handle the WEC motion, it was crucial to maintain a fine and equally-sized mesh between the fixed and overset parts to prevent any conservation problems between the meshes. This was accomplished by utilizing an overlapping mesh region. The Volume of Fluid method was used in the current study to identify the free surface. The two-phase media (air and water) and their interface are recognized and explained briefly as follows. A scalar function called the volume fraction was utilized to describe the control volume. If the volume fraction equals zero, it indicates the presence of air, while a value of one indicates the presence of water. When the cells contain an interface between zero and one, it is identified as the free surface.

4.2. Pitch response amplitude operators

In this paper, the hydrodynamic behavior of an asymmetric WEC model optimized in the sea to the west of Jeju island induced by regular waves was investigated numerically and experimentally. The following conclusions are drawn from the comparison of the nonlinear hydrodynamic behavior of the asymmetric WEC at different incident wave heights based on the model experiment as well as the comparison of the hydrodynamic coefficients due to the forced pitch oscillation with different motion amplitudes obtained with the OpenFOAM model based on a RANS solver and the WAMIT model based on linear potential theory. Fig. 5 shows a comparison between the experimental pitch RAO due to different incident wave amplitudes ($H = 0.01$ and $0.03\,m$) and the numerical results calculated with OpenFOAM and WAMIT. All the results show a resonance phenomenon in which the motion increases sharply when the incident period (T) of the incoming wave coincides with the natural period (T_N) of the asymmetric WEC. However, the results with WAMIT based on the linear potential theory is highly over-predicted near the natural period (T_N). The OpenFOAM results agree well with the experimental results except for the relatively longer wave period. In the experiment, it was difficult to observe steady-state periodic pitch motion longer than the natural period (T_N) since the wave reflected from the asymmetric WEC was re-reflected at the wave maker and then disturbed the pitch excursion. The experimental and numerical results show that the pitch RAO decreases as the height of the incident wave increases. This result will be analyzed in detail through the following spectral analysis.

In order to compare the time series of pitch excursion due to different incident wave heights ($H = 0.01$ and $0.03\,m$) at the natural period (T_N), the results corresponding to three wavelengths of the incident wave are shown in Fig. 6 (top). The figure shows that the numerical results predict the experimental results well. As the wave height increases, the amplitude of the pitch excursion increases. The clockwise (positive) pitch excursions are larger than the counterclockwise (negative) pitch excursions as the paunch part of the asymmetric WEC is designed so that the hydrodynamic force induced by the incident particle velocity profile increases clockwise pitch motion. Moreover, the non-linear pitch excursion behavior of the asymmetric WEC is further amplified with an increase in wave height, but reduced as wave height decreases. The nonlinear behavior that was observed is consistent with what was anticipated, owing to the distinct configuration of the paunch part of the asymmetric WEC and its interaction with the incoming waves. Fig. 6 (bottom) shows a comparison of the pitch excursion amplitude through spectral analysis. In the spectral analysis of the case where the wave height is the highest, the primary pitch amplitude ($f_p = 0.625\ [1/s]$) and the second harmonic term ($f_h = 1.25\ [1/s]$) are higher and the third harmonic ($1.875\ [1/s]$) newly appears (Fig. 6). Due to the increase of the primary harmonic amplitude and the presence of higher harmonics as a nonlinear effect, the pitch amplitude is 2.5 times larger although the height of the incident wave is increased by three times. This can be explained by the fact that in the case of high wave height the RAO becomes smaller than that in the case of low wave height.

4.3. Wave excitation moment (fixed body)

Wave excitation moments (X_5) were numerically calculated by integrating the dynamic pressure and shear stress induced by regular waves over the asymmetric WEC in fixed mode (without a dynamic mesh motion). Fig. 7 shows a comparison of the wave exciting moment non-dimensionalized by the water density, gravitational acceleration, wave amplitude, and the submerged section area and breadth of the

asymmetric WEC between WAMIT and OpenFOAM with different wave heights. The OpenFOAM results are slightly overestimated at relatively long wave periods. Overall, the two numerical results agree well with each other since in these cases wave steepness ($ka \leq 0.039$) is small.

4.4. Radiation moment (oscillating body)

The forced oscillation motion of the asymmetric WEC in single-pitch mode was simulated to investigate the role of hydrodynamic forces in the nonlinear dynamic behavior induced by the following equation:

$$\theta_5 = a_5 \sin(\omega t) \tag{4}$$

where a_5 and ω are the motion amplitude and the angular frequency for the forced oscillation in pitch mode, respectively.

The time series of the radiation moment in pitch mode (M_{55}) was calculated based on the dynamic pressure on the asymmetric WEC. The real part ($Re\{\bullet\}$) and imaginary part ($Im\{\bullet\}$) were separated from the time series by conversion to the frequency domain using a Fourier series transform as follows:

$$Re\{M_{55}(\omega)\} = \frac{2}{T}\int_t^{t+T} M_{55}(t)\cos(\omega t)dt \tag{5}$$

$$Im\{M_{55}(\omega)\} = \frac{2}{T}\int_t^{t+T} M_{55}(t)\sin(\omega t)dt \tag{6}$$

The added moment of inertia (a_{55}) and damping (b_{55}) coefficients in pitch mode were determined as follows:

$$a_{55} = \frac{Im\{M_{55}(\omega)\}}{a_5\omega^2} \tag{7}$$

$$b_{55} = \frac{Re\{M_{55}(\omega)\}}{a_5\omega} \tag{8}$$

In this study, the motion amplitudes $a_5 = 0.10, 0.20,$ and 0.40 rad and the motion angular frequencies $\omega = 2, 4, 6, 8,$ and 10 rad/ s were forced to sinusoidal pitching motions of the asymmetric WEC. All the results were numerically calculated with OpenFOAM. The results for added moment of inertia and radiation damping with different oscillating amplitudes were compared to the results obtained using WAMIT and presented with angular motion period in seconds, as shown in Fig. 8. This comparison was not only intended to clarify the nonlinear hydrodynamic effects, as the forced motion amplitude is increased, but also to show that the reliability of the results obtained with OpenFOAM is comparable to the reliability of the results obtained using WAMIT. All of the values are non-dimensionalized by the width (B) and the submerged section area (A) of the asymmetric WEC. The OpenFOAM results due to lower amplitude motions ($a_5 = 0.10$ and 0.20) agree well with the WAMIT results. However, the hydrodynamic coefficients due to the highest motion amplitude are mostly over-estimated by OpenFOAM. The difference between the WAMIT and OpenFOAM results will be analyzed in detail through the following spectral analysis.

Fig. 9 shows a comparison of the radiation moment time series and spectral analysis of radiation moment due to the forced oscillation with different motion amplitudes ($a_5 = 0.1, 0.2,$ and 0.4 rad) and $\omega = 10\ rad/s$. The time series of radiation moment with the lowest amplitude has a linear sinusoidal form, whereas the time series of radiation moment with the highest amplitude has a strongly nonlinear form. This result is clearly observable from the spectral analysis. A comparison of the spectral analyses for radiation motion (see Fig. 11) shows that the primary harmonic moment term ($f_p = 1.59\ [1/s]$) and higher harmonic terms are also stronger and newly appeared, respectively, in the case at higher amplitude ($a_5 = 0.4$ rad). The increase of nonlinearity is considered to be a major factor in the difference between the results of the linear potential flow solution (WAMIT) and the results of the OpenFOAM solution shown in Fig. 8.

In order to further investigate the nonlinearities of radiation moment, instantaneous snapshots of the vorticity field about the z-axis, and the dynamic pressure distribution and the wave surface elevation at the maximum and minimum moment due to the forced oscillation were compared for different motion amplitudes, as shown in Figs. 10 and 11, respectively. As the highest motion amplitude, vorticities are strongly formed at both the front and rear sides of the asymmetric WEC along the width axis. Moreover, the higher the dynamic pressure distribution over the wider surface at the front of the WEC, the higher the motion amplitude. It was also found that in the three-dimensional numerical results the dynamic pressure distribution is concentrated in the middle of the width axis of the asymmetric WEC. This phenomenon was not predicted by the two-dimensional (pseudo-three-dimensional in FVM) numerical model. Furthermore, as the oscillating motion of the WEC is counter-clockwise (nodding-down), a positive dynamic pressure is produced and the vorticity distribution is similar to a steady flow from downstream to upstream passing through the asymmetric WEC; meanwhile, as the oscillating motion of the WEC is clockwise (nodding-up) a negative dynamic pressure is produced and the vorticity distribution is similar to a steady flow from upstream to downstream passing through the asymmetric WEC [36], as shown in Figs. 10 and 11, respectively. These results indicate that the highest motion amplitude affects the nonlinearity of the radiation moment of the asymmetric WEC to a greater degree.

5. Conclusions

This paper studies the hydrodynamic behavior of an asymmetric WEC model, which has been optimized in the sea to the west of Jeju island, under the influence of regular waves. Both numerical and experimental methods were utilized in this investigation. The nonlinear hydrodynamic behavior of the asymmetric WEC at different incident wave heights was compared based on a model experiment. In addition, the hydrodynamic coefficients due to forced pitch oscillations with different motion amplitudes were compared using two models: the OpenFOAM model based on a RANS solver, and the WAMIT model based on linear potential theory. In order to minimize the numerical uncertainty of OpenFOAM, a grid convergence test was conducted to investigate wave generation and propagation. The accuracy of the numerical results was validated by comparing them with the experimental results. Based on the findings of this study, the following conclusions can be drawn.

- The study revealed that the pitch RAO exhibited a decrease at high incident wave heights, as supported by both experimental data and OpenFOAM results. Additionally, spectral analysis confirmed that as the wave height increased, the decrease in RAO was attributed to the rise in the nonlinear component of the higher-order term of pitch motion.
- The hydrodynamic coefficients and wave excitation were determined separately using a linear solution approach, while taking into account the nonlinear viscous effect. This allowed for the consideration of nonlinear dynamic behavior. The wave excitation moments obtained from OpenFOAM were in good agreement with those obtained from WAMIT, as the incident wave exhibited almost linear characteristics (i.e., $ka \leq 0.039$).
- Forced pitch oscillations of the WEC with lower motion amplitudes result in hydrodynamic coefficients that are in good agreement with solutions from both OpenFOAM and WAMIT. However, when motion amplitudes are higher, a difference in results is observed between OpenFOAM and WAMIT. This distinction has been attributed to the strong nonlinear effects, which have been confirmed through spectral analysis.
- Furthermore, it was found that the highest motion amplitude causes a strong vorticity and increased dynamic pressure near the asymmetric WEC, which in turn causes the nonlinearity effect to

strengthen. Thus, it can be inferred that the radiated motion of the asymmetric WEC is largely dominated by the nonlinear effect.

Funding source

This work was supported by the National Research Foundation of Korea (NRF) grant funded by the Korea government (MSIT). (No. 2021R1A2C1014600). This work was also supported by Basic Research Program through the National Research Foundation of Korea (NRF) funded by the Ministry of Education (No. 2022R1I1A1A01069442).

CRediT authorship contribution statement

Haeng Sik Ko: Conceptualization, Methodology, Formal analysis, Investigation, Writing – original draft. **Sunny Kumar Poguluri:** Software, Writing – review & editing, Funding acquisition. **Jeong-Heon Shin:** Validation, Investigation. **Yoon Hyeok Bae:** Supervision, Project administration, Funding acquisition.

Declaration of competing interest

The authors declare that they have no known competing financial interests or personal relationships that could have appeared to influence the work reported in this paper.

Acknowledgments

This work was supported by the National Research Foundation of Korea (NRF) grant funded by the Korea government (MSIT). (No. 2021R1A2C1014600). This work was also supported by Basic Research Program through the National Research Foundation of Korea (NRF) funded by the Ministry of Education (No. 2022R1I1A1A01069442).

References

[1] P.A. Lynn, Electricity from Wave and Tide: an Introduction to Marine Energy, John Wiley & Sons, Chichester, UK, 2013.
[2] M.E. McCormick, Ocean Wave Energy Conversion, Dover Publications, Inc, NY, US, 2007.
[3] S.H. Salter, Wave power, Nature 249 (1974) 720–724.
[4] S.H. Salter, D.C. Jeffrey, J. Taylor, First Year Interim Report on Edinburgh Wave Power Project: Study of Mechanism to Extract Power from Sea Waves, University of Edinburgh, 1975, September. Technical report, Wave-Power project.
[5] D.V. Evans, A Theory for wave-power absorption by oscillating bodies, J. Fluid Mech. 77 (1976) 1–25.
[6] A. Pecher, J.P. Kofoed, T. Larsen, The Extensive R&D behind the Weptos WEC. RENEW2014, 2014, pp. 351–358.
[7] D. Kim, S.K. Poguluri, H.S. Ko, H. Lee, Y.H. Bae, Numerical and experimental study on linear behavior of salter's duck wave energy converter, Journal of Ocean Engineering and Technology 33 (2) (2019) 116–122.
[8] Y. Liu, S. Yoshida, C. Hu, M. Sueyoshi, L. Sun, J. Gao, P. Cong, G. He, A reliable open-source package for performance evaluation of floating renewable energy systems in coastal and offshore regions, Energy Convers. Manag. 174 (2018 Oct 15) 516–536.
[9] Y.H.A.M.S. Liu, A frequency-domain preprocessor for wave-structure interactions—theory, development, and application, J. Mar. Sci. Eng. 7 (3) (2019 Mar 26) 81.
[10] H. Asmuth, P. Schmitt, B. Elsaesser, A. Henry, Determination of non-linear damping coefficients of bottom-hinged oscillating wave surge converters using numerical free decay tests, in: Proceedings of the 1st International Conference on Renewable Energies Offshore, 2014, pp. 24–26. Lisbon, Portugal.
[11] B. Devolder, P. Rauwoens, P. Troch, Numerical simulation of a single floating point absorber wave energy converter using OpenFOAM, Progress in Renewable Energies Offshore (2016) 197–205. CRC Press: Boca Raton, FL, USA.
[12] S.K. Poguluri, I.H. Cho, Y.H. Bae, A Study of the hydrodynamic performance of a pitch-type wave energy converter–rotor, Energies 12 (5) (2019) 842.
[13] H.S. Ko, I.H. Cho, Y.H. Bae, Numerical and experimental study of a horizontal cylinder-type wave energy converter with off-centered axes of rotation, Int. J. Offshore Polar Eng. 29 (4) (2019) 429–436 (a).
[14] A.S. Zurkinden, F. Ferri, S. Beatty, J.P. Kofoed, M.M. Kramer, Non-linear numerical modeling and experimental testing of a point absorber wave energy converter, Ocean Eng. 78 (2014) 11–21.
[15] G. Giorgi, J.V. Ringwood, Consistency of viscous drag identification tests for wave energy applications, in: Proceedings of the 12th European Wave and Tidal Energy Conference (EWTEC), vol. 27, 2017. Cork, Ireland.
[16] H. Gu, P. Stansby, T. Stallard, E.C. Moreno, Drag, added mass and radiation damping of oscillating vertical cylindrical bodies in heave and surge in still water, J. Fluid Struct. 82 (2018) 343–356.
[17] M. Lawson, Y.H. Yu, A. Nelessen, K. Ruehl, C. Michelen, Implementing nonlinear buoyancy and excitation forces in the wec-sim wave energy converter modeling tool, V09BT09A043, in: InInternational Conference on Offshore Mechanics and Arctic Engineering vol. 45547, American Society of Mechanical Engineers, 2014 Jun 8.
[18] H. Wang, A. Somayajula, J. Falzarano, Z. Xie, Development of a blended time-domain program for predicting the motions of a wave energy structure, J. Mar. Sci. Eng. 8 (1) (2019 Dec 19) 1.
[19] G. Giorgi, S. Sirigu, M. Bonfanti, G. Bracco, G. Mattiazzo, Fast nonlinear Froude–Krylov force calculation for prismatic floating platforms: a wave energy conversion application case, Journal of Ocean Engineering and Marine Energy 7 (4) (2021 Nov) 439–457.
[20] S. Chandrasekaran, V.V. Sricharan, Numerical analysis of a new multi-body floating wave energy converter with a linear power take-off system, Renew. Energy 159 (2020 Oct 1) 250–271.
[21] C. Eskilsson, J. Palm, J.P. Kofoed, E. Friis-Madsen, CFD Study of the Overtopping Discharge of the Wave Dragon Wave Energy Converter, Renewable Energies Offshore, 2015, pp. 287–294.
[22] P. Schmitt, B. Elsaesser, On the Use of OpenFOAM to model oscillating wave surge converters, Ocean Eng. 108 (2015) 98–104.
[23] H.S. Ko, D. Kim, S.K. Poguluri, I.H. Cho, Y.H. Bae, Optimal performance studies of a horizontal eccentric cylinder-type WEC in western sea of Jeju island with linear inviscid and nonlinear viscous numerical model, Ocean Eng. 202 (2020), 107180.
[24] J.H. Vugts, The hydrodynamic coefficients for swaying, heaving and rolling cylinders in a free surface, Int. Shipbuild. Prog. 15 (167) (1968) 251–276.
[25] L. Bonfiglio, S. Brizzolara, C. Chryssostomidis, Added mass and damping of oscillating bodies: a fully viscous numerical approach, Recent Advances in Fluid Mechanics, Heat & Mass Transfer and Biology (2011) 210–215.
[26] J. Davidson, S. Giorgi, J.V. Ringwood, Linear parametric hydrodynamic models for ocean wave energy converters identified from numerical wave tank experiments, Ocean Eng. 103 (2015) 31–39.
[27] H.S. Ko, D. Kim, I.H. Cho, Y.H. Bae, Numerical and experimental study for nonlinear dynamic behavior of an asymmetric wave energy converter, in: The 29th International Ocean and Polar Engineering Conference, International Society of Offshore and Polar Engineers, Hawaii, 2019 (b).
[28] S.K. Poguluri, Y.H. Bae, A study on performance assessment of WEC rotor in the Jeju western waters, Ocean Systems Engineering 8 (4) (2018) 361–380.
[29] S.K. Poguluri, I.H. Cho, Y.H. Bae, A study of the hydrodynamic performance of a pitch-type wave energy converter–rotor, Energies 12 (5) (2019) 842.
[30] S.K. Poguluri, D. Kim, H.S. Ko, Y.H. Bae, Performance analysis of multiple wave energy converters due to rotor spacing, Journal of Ocean Engineering and Technology 35 (3) (2021) 229–237.
[31] S.K. Poguluri, H.S. Ko, Y.H. Bae, CFD investigation of pitch-type wave energy converter-rotor based on RANS simulations, Ships and Offshore Structures 15 (10) (2020) 1107–1119.
[32] C.H. Lee, J.N. Newman, Computation of Wave Effects Using the Panel Method. Numerical Models in Fluid–Structure Interaction, MIT press, Cambridge, MA, 2005, pp. 211–251.
[33] V. Yakhot, S.A. Orszag, S. Thangam, T.B. Gatski, C.G. Speziale, Development of turbulence models for shear flows by a double expansion technique, Phys. Fluid. Fluid Dynam. 4 (7) (1992) 1510–1520.
[34] P. Higuera, J.L. Lara, I.J. Losada, Realistic wave generation and active wave absorption for Navier-Stokes models, application to OpenFOAM, Coast. Eng. 71 (2013) 102–118.
[35] H.A. Schaffer, G. Klopman, Review of multidirectional active wave absorption methods, J. Waterw. Port, Coast. Ocean Eng. 126 (2) (2000) 88–97.
[36] J. Wu, Y. Yao, D. Sun, Z. Ni, M. Göteman, Numerical and experimental study of the solo duck wave energy converter, Energies 12 (10) (2019) 1941.